Composites: Part A 73 (2015) 116–124

Contents lists available at ScienceDirect

Composites: Part A

journal homepage: www.elsevier.com/locate/compositesa

Multiscale tool–fabric contact observation and analysis for composite fabric forming

Olga Smerdova [1], Michael P.F. Sutcliffe *

Department of Engineering, University of Cambridge, Trumpington Street, Cambridge CB2 1PZ, UK

ARTICLE INFO

Article history:
Received 18 December 2014
Received in revised form 3 March 2015
Accepted 5 March 2015
Available online 13 March 2015

Keywords:
A. Carbon Fibre
A. Fabrics/textiles
E. Forming
Friction

ABSTRACT

This paper provides measurements and analysis at the meso and microscopic scales of the real contact area between twill carbon fabric and a flat glass counterface. The mesoscopic contact area associated with tow contacts is about 55–75% of the nominal area. However, the total real contact length within the tow contacts, associated with microscopic contact at the fibre level, is only 4–8% of the idealised contact conditions with parallel touching fibres, for a nominal contact pressure of around 2 kPa. The dependence of real contact area on fabric shear angle is also investigated. The estimated real contact pressure is 15,000 times higher than the nominal contact pressure. Models or experiments of friction in composites forming which do not take into account the real contact situation, which is very far from an idealised packing arrangement, may fail to capture the essential tribological mechanisms.

1. Introduction

Shear is the main deformation mechanism in textile forming, independently of forming process and fabric type [1–3]. As a textile is formed into a curved shape, the shear angle varies locally over the part, reaching a maximum shear angle of up to 60° [4]. This is the case for dry or pre-impregnated woven and non-crimp fabrics with any type of polymer binder. In many composite forming processes, internal shear deformation occurs in conjunction with a compression load applied by a metal or rubber tool, which is used either to give the composite part the desired shape before filling it with resin or to reduce the voids between already-impregnated prepregs. As well as internal fabric shear, there may be gross sliding between the tool and fabric and between plies in a multi-ply stack, with details depending on the composite architecture and processing method. During the forming process, friction between the composite ply and the tool, and between composite plies, may play an important role in shaping the part and may also affect the formation of local defects such as wrinkling in the composite part.

Textile shear behaviour at the macro and mesoscopic scales is usually investigated either by bias extension or picture frame tests [5–10]. Shear characteristics obtained by these tests or by virtual experiments [11,12] are used in textile forming simulations. Most of the numerical modelling work presents the fabric either as a macroscopic deformable solid without details of the internal structure, or as a set of woven tows defined at the mesoscopic scale [13–19]. There are only a few numerical models which regard composite fabric as composed of individual fibres at the microscale [20,21]. Due to the computational cost, the tows contain only a relatively few fibres, far from the situation of real fabrics with thousands of fibres in a tow. Mesoscopic models seem the most promising approach, as they represent a compromise between the time of computation and the accuracy of representation of internal deformation. The mesoscopic contact area between tows and a tool is one of the results provided by such models. At this scale, each tow/tool contact spot is of the order of tens of square millimetres, and the total ply/tool contact area is composed of many of these mesoscopic contact spots. It is generally assumed that, since each tow is densely packed with fibres, each mesoscopic contact spot is fully filled with fibre micro-contacts [11,13,16,29,33,38–40]. However, to our knowledge, this hypothesis has not been verified. The experimental work presented in the current paper enables verification of whether this widely accepted hypothesis is correct and, therefore, will contribute to the further improvement in accuracy of composite forming simulations.

A number of experiments have been done to measure friction between fabric and a metal tool [22–31]. The friction force is usually measured while sliding a large piece of fabric against a metal

* Corresponding author. Tel.: +44 (0)1223 332996.
E-mail addresses: Olga.smerdova@eng.cam.ac.uk, olga.smerdova@ensma.fr (O. Smerdova), mpfs@eng.cam.ac.uk (M.P.F. Sutcliffe).
[1] Present address: Institut Pprime, ISAE-ENSMA, 1 avenue Clément Ader 86961 Futuroscope, France.

http://dx.doi.org/10.1016/j.compositesa.2015.03.009
1359-835X/

counterface, and the friction coefficient is defined for the whole apparent contact surface. This approach does not represent composite forming accurately for two reasons. Firstly, there is an ambiguity associated with the ply/tool friction term. While the friction force measured in these experiments is due to sliding friction between two macroscopic continuous solids, in real forming of curved composite parts most of the frictional energy is dissipated by local ply/tool friction due to shear. The former friction type is characteristic for the fabric/blank holder relationship. By contrast, the latter friction type is relevant for the moulded area which undergoes high shear deformation under the compression force applied by the tool. This latter type of friction is very different from the fabric/tool sliding friction and needs to be understood to model accurately forming of these materials.

Secondly, in order to understand and to model friction-related phenomena accurately, ply/tool contact should be investigated at the microscopic level. The understanding gained from such an approach can also inform design and characterisation of appropriate experiments. As far as we know, the real contact area in fabric/tool contact has not previously been measured. The real contact area between solids is often much smaller than the apparent one and depends on the surface topography, material and normal load. For instance, the ratio between real and apparent contact areas for metal/metal contact is typically about 0.5×10^{-6} under a normal pressure of 1.4 kPa [32]. On the other hand, for the contact of two elastomers, this ratio can be close to 1. Recently, a contact model for fabric/tool friction was introduced [33], which looks at the influence of roughness on the metal tool on friction in fabric forming. Considering contact at the mesoscopic level, this model uses an assumption of an idealised packing of parallel touching fibres within each tow/tool contact spot. However, this critical assumption has not been verified. Moreover, high shear deformation of fabrics during forming induces dramatic surface changes, as seen by the naked eye and through microscope observation [34,35]. Does the real contact area and local friction change during shear due to these mesoscopic tow deformations?

In this paper, we will present a methodology to investigate microscopic fabric/tool contact under shear loading, and apply this to the forming of twill fabric. The aim of this study is to bridge the gap between modelling of fabric forming and real forming processes and to provide experimental data of real contact area in fabric forming that can be used in modelling simulations. To do so, we use a novel experimental rig and method described in detail in Ref. [36]. In particular, Ref. [36] presents an analysis of the deformations and forces applied by the experimental rig, discusses the similarities and differences of this method comparing to the classical shear experiments, and describes an image analysis algorithm used to extract the images of fibre contact. The focus of the current paper is to take this method for identifying contacting fibres and use this in a multiscale analysis of composite fabric/tool contact under shear loading.

This paper studies tool/fabric contact of dry twill carbon fabric, representing the pre-forming step for a resin transfer moulding process. The contact pressure used here is of the order of real forming pressures applied to the fabric in a highly deforming area, where shear takes place during the pre-forming process. The method presented works for contact between a glass plate and carbon fibres and can be used for any carbon fibre composite architecture (UD, fabric, NCF, 3D...). Moreover, wet contact of carbon fabric impregnated with polymer matrix can also be studied by the method presented. In principle, a contact with other optically reflective fibres can be measured using the same technique if the optical properties and thickness of the semi-reflective coating are adjusted. The use of glass as a counterface is imposed by the combination of transparency and hardness of this media. Curvature of the glass plate could be introduced to simulate a curved mould, but this would require correction of the associated contact image distortion.

2. Materials & methods

2.1. Experimental method

This paper uses a micromechanical experimental rig which has been developed to investigate composite forming behaviour at the microscopic scale. The details of the rig and the methods used to identify individual fibre contacts are given in [36], and here we give a brief overview. The loading rig is illustrated in Fig. 1. A key feature of the rig is the ability to observe the evolution of microscopic contacts under simultaneous application of shear and compression loadings. A composite fabric sample of size $80 \times 80\ mm^2$ is compressed via a screw-spring arrangement between two glass plates with a gauge area of $45 \times 20\ mm^2$. Two linear motors pull the fabric in opposite directions at ±45° to the tow orientations, thereby increasing the shear angle between crossing tows. An open shear frame is used to clamp the specimen and connect it to the motors. The rig is placed under an optical microscope equipped with a camera.

A semi-reflective optical coating was deposited on one of the glass plates to enable direct contact observations. Such a coating is often used in tribological experiments to measure the thickness of lubrication films in ball/disc sliding contacts. The optical film has two layers, a base layer of chromium and a top layer of silica in contact with the fabric sample. The thicknesses of both layers (140 nm for the SiO_2 and 8 nm for the Cr) were optimised for our application in order to obtain the best contrast of carbon fibre contacts. A Matlab algorithm to analyse the obtained images and detect fibre contacts was developed and described in Ref. [36]. In brief this uses a combination of filtering and thresholding to identify bright, elongated features corresponding to the fibre contacts. The algorithm scans an image which contains clearly visible bright contact areas and detect lines corresponding to fibre contacts. There is insufficient image resolution to measure accurately the width of individual fibre contacts, so only the length of the fibre contacts is measured by the algorithm, enabling a calculation of the total contact length in the image. Because of the clear contrast produced by the optical film, identification of contacts is a relatively straightforward and unambiguous process. Several coated

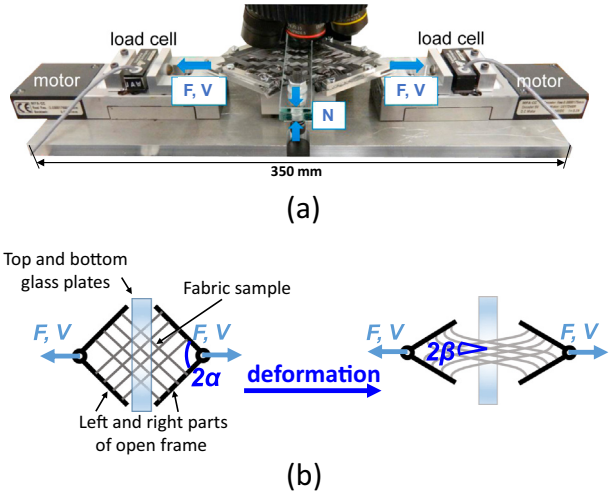

Fig. 1. Experimental rig: (a) photograph; (b) deformation schema.

glass plates were prepared in case wear of the coating becomes noticeable. However, only a few scratches appeared on the surface, which did not affect the efficiency of the image processing algorithm.

To obtain a representative area of the fabric, it is necessary to observe an area comprising at least several tows and their cross-overs. Therefore, several adjacent images were taken at an appropriate resolution to identify the individual fibre contacts and then patched together to give a larger area which allows multiscale examination of the fabric deformation. When the microscopic measurements were complete for one configuration, the spacing between the two motors was increased to induce further fabric shearing, and the imaging was repeated.

2.2. Materials

The method outlined above can be used to analyse fabric/tool contact for a wide range of composite materials and architectures. In this paper, we present experimental results obtained for one composite fabric which was used to develop and validate the proposed method. This is a 2 × 2 twill-woven T700 carbon fibre fabric with 24 K tows and without binder, having an areal density of 400 gsm. A square sample of 80 × 80 mm^2 area was cut from a fabric roll. The tows 20 mm away from the sample centre were removed leaving the central square woven area of 40 × 40 mm^2. This was done to minimise friction between tows outside the clamped area between the glass plates. The specimen was clamped into the open shear frame so that the tows run parallel to the frame sides.

The glass plates used to compress the fabric were made from heat-toughened soda lime float glass. They had a surface average roughness of $R_a = 0.0082 \pm 0.0003$ μm and $R_q = 0.0104 \pm 0.0005$ μm as measured with a contact profilometer (Form Talysurf 120, Taylor Hobson, Leicester, UK).

2.3. Experimental conditions

Three micromechanical quasi-static experiments were carried out for the validation of the experimental method. Firstly, a composite fabric specimen was sheared under the weight of the top glass plate without any additional compressive loading. Lateral motion of the glass plates was restricted by the loading screws running through the glass plates. The applied normal load in this case was equal to 0.23 N, corresponding to a nominal contact pressure of 0.26 kPa. Then, a similar experiment was carried out under a compression load of 1.77 N. This load corresponds to a normal pressure of 1.9 kPa on the total compressed fabric area at the beginning of the test. Finally, the repeatability of the experiments was verified by repeating the experiment at a compressive load of 1.77 N. The contact area images were taken with 5–6 regular displacement steps. All the experiments presented in this paper were performed at room temperature and humidity. Thus, several shear cycles of loading and unloading were done on the same specimen before the tests whose results are presented here. At the end of each experiment, the specimen was returned to its initial state and the compression load removed. The same specimen was used for two loading conditions to allow the comparison of contact area between different tests.

2.4. Glossary of image analysis results

Various parameters can be extracted from an image of the real microscopic contact of a composite fabric. In this section, we define the parameters used and outline how they are measured.

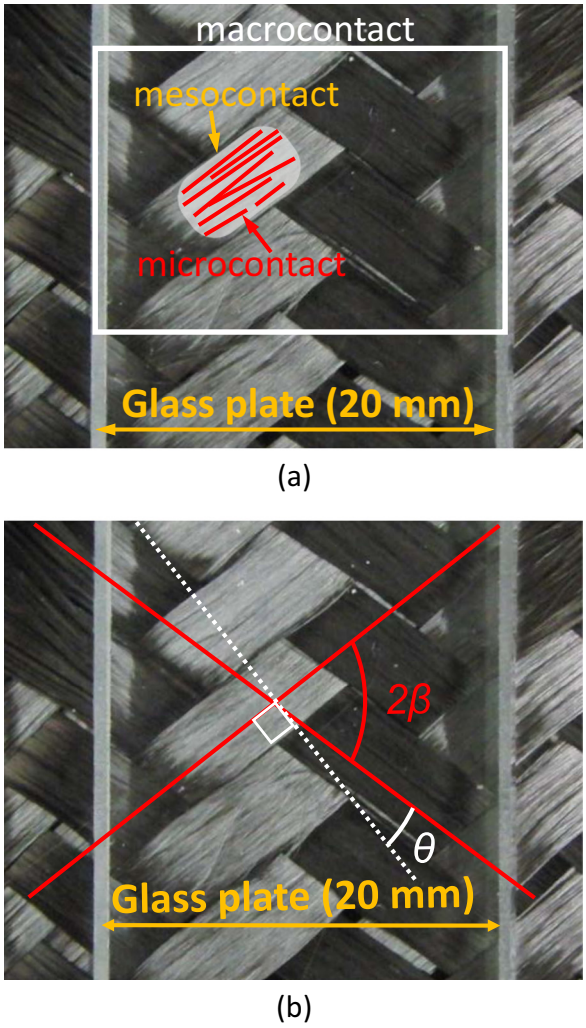

Fig. 2. (a) Macro-, meso- and micro-contact areas and (b) shear angle θ definitions.

Three *scale* definitions – macroscopic, mesoscopic and microscopic – are shown in Fig. 2(a), following the established terminology [13], i.e. macroscopic deals with the deformed shape of the composite fabric, mesoscopic is at the scale of the tows and microscopic is at the scale of the fibres.

Apparent contact area A_{app}/pressure p_{app} are related to the whole sample area clamped between the two glass plates.

Microscopic shear angle θ_{mic} is calculated as $90° - 2\beta$, where the tow cross-over angle 2β is the difference in orientation of the opposing sets of tows, as illustrated in Fig. 2(b). This shear angle is termed microscopic, because in the analysis the orientations of tows is derived from all the local fibre contacts making up each tow contact.

Macroscopic contact area A_{mac} is the total area examined under the microscope (termed "macrocontact" in Fig. 2(b)). In subsequent analysis, the area of an array of 8 × 9 images taken with an optical magnification of 5× is considered. This represents an apparent contact area of 19.33 × 16.31 mm^2.

Mesoscopic contact area A_{mes} is the area inside the envelope curve for all local fibre contacts within a given tow. It can be viewed as the apparent contact area for a tow.

Microscopic contact length L_{mic} and area A_{mic}: The microscopic contact length L_{mic} is a sum of the lengths of each of the local fibre contacts within the macrocontact A_{mac}, while A_{mic} is the corresponding area of contact.

3. Results & discussions

The experimental method provides images of the local fibre contacts over the observation area A_{mac}. This area was chosen so that at least four whole tow contacts can be observed at each step of the deformation.

An example of part of the macroscopic observation area, including one whole tow contact, is presented in Fig. 3. The micro-contact of individual fibres for this tow is clearly seen, along with the mesoscopic boundaries of the tow contact. Not all the fibres are aligned in the same direction, but the orientation of most of them coincides with the overall tow orientation.

Fig. 4 presents the fibre contact patches over the whole macroscopic area A_{mac} for five deformation steps with each of the three experiments. The change in shear angle is clearly visible from the contact patch geometries. Changes in the density of local fibre contacts within each tow, as well as the area of the tows, will be quantified at the micro and mesoscopic scales in the following sections.

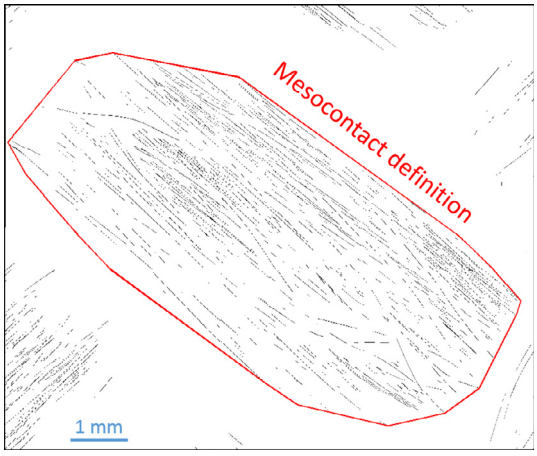

Fig. 3. Real area of fibre contact for a complete tow contact at the beginning of the first test with a compressive load of 1.77 N.

3.1. Mesoscopic analysis

The overall contact patches presented in Fig. 4 show that all tows elongate longitudinally and shrink transversally with increasing shear angle. The mesoscopic contact area A_{mes}, which is defined as the envelope of all local fibre contacts within a tow, is determined by finding the convex hull using a standard Matlab analysis function, as illustrated in Fig. 3.

Fig. 5 shows the variation with shear angle θ of the average value of the mesoscopic contact area A_{mes} for the four tows in each macroscopic area A_{mac}, for all three microscopic measurements. Error bars show the standard deviation of the four tows within each set of measurements. Note that the fabric shear angle is determined from the microscope analysis; details are given below. This plot shows that A_{mes} is roughly independent of the fabric shear. This result is not obvious, taking into account the way that the shape of each mesoscopic contact changes significantly during deformation. Apparently the effects of longitudinal elongation and transversal shrinkage of the tows approximately cancel each other. The higher normal load gives a higher mesoscopic contact area. However, the repeated deformation and loading with the same sample could also be a reason for part of this increase, as indicated by the difference between the two experiments with a compressive load of 1.77 N. As the deformation is repeated, it appears that the carbon tows become more compliant and deform more easily, which may lead to a larger contact area.

A mesoscopic contact density D_{mes}, which gives an effective contact area ratio for the tows, is defined as the ratio of the area of the N tow contact envelopes defining the mesoscopic contact area to the corresponding total nominal contact area A_{mac} as follows:

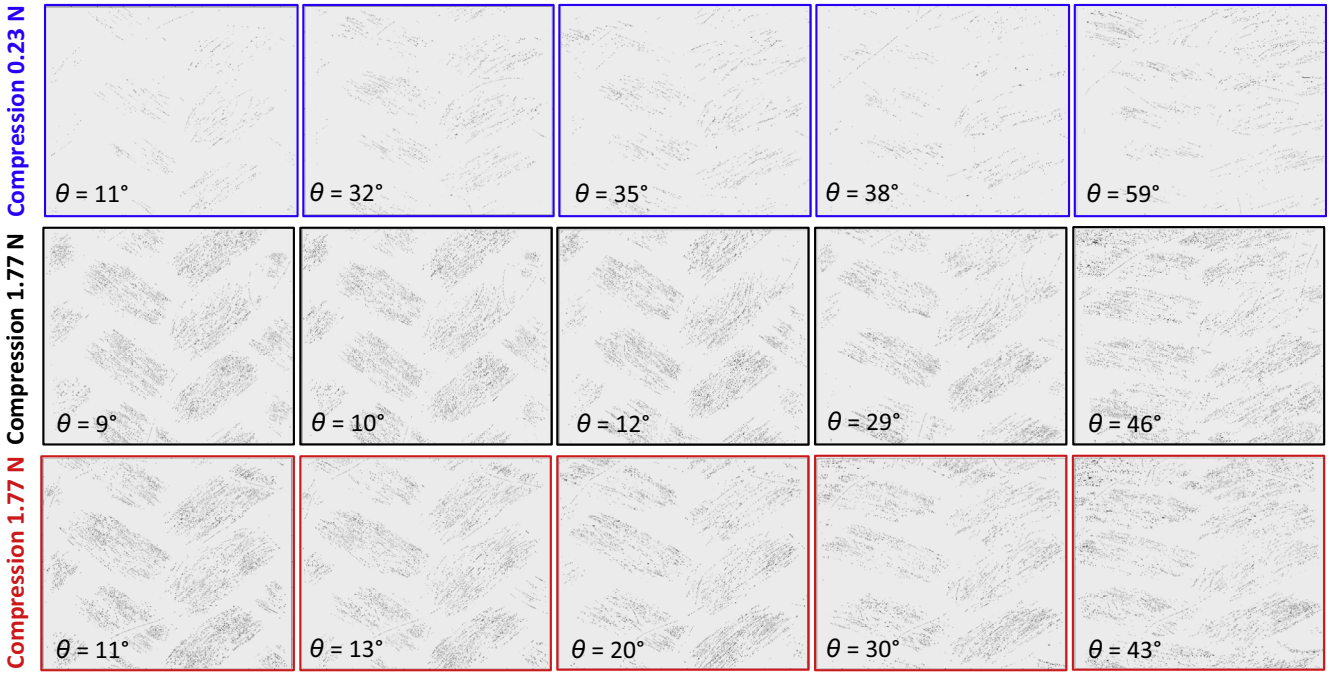

Fig. 4. Contact area patterns for the macroscopic area A_{mac} used in the analysis.

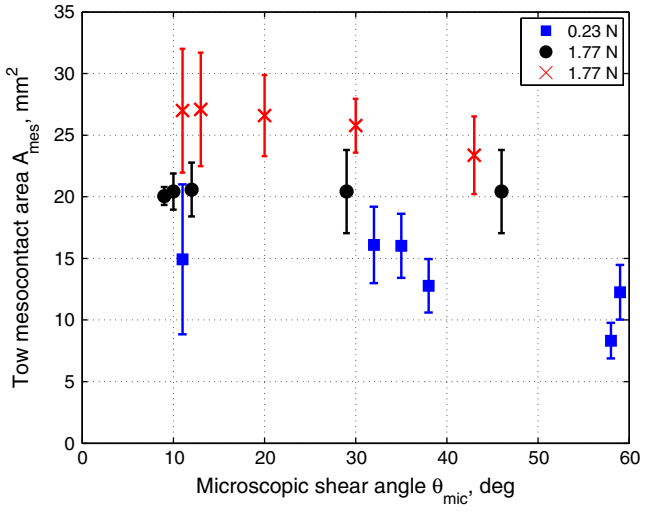

Fig. 5. Effect of fabric shear on the tow meso-contact area. Error bars represent the standard deviation of the four values of the tow meso-contact area within the overall analysis area A_{mac}.

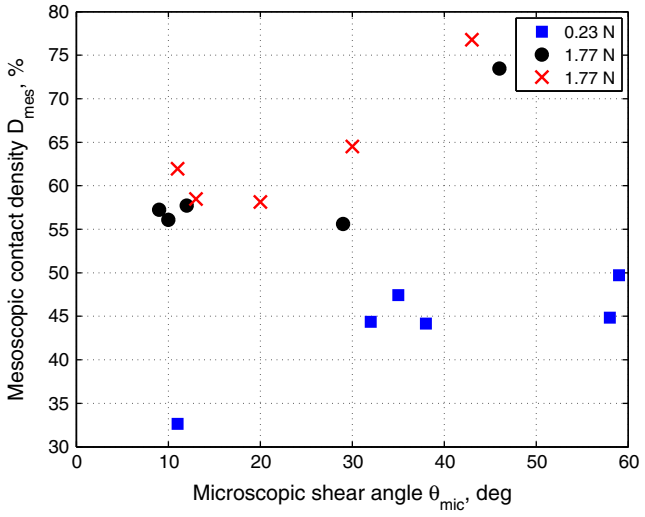

Fig. 6. Evolution of mesoscopic contact density with shear angle.

$$D_{mes} = \frac{\sum_{i=1}^{N} A_{mes,i}}{A_{mac}} \times 100\% \quad (1)$$

The variation of mesoscopic contact density (expressed as a percentage) with fabric shear angle is presented in Fig. 6. As expected, the contact density is higher for the higher load. The mesoscopic contact density is constant at lower shear angles up to a shear angle of about 30° and then increases significantly with increasing shear angle in both tests.

In general, the contact density at this mesoscale is rather high, i.e. 55–75% for the 1.77 N compressive load and 35–50% for the load of 0.23 N. These values can be compared with the values presented by [37] for a balanced 5HS satin carbon fabric. Applying apparent contact pressures of 20, 60 and 100 kPa, this paper reported measured mesoscopic contact densities of 24%, 39% and 45%, respectively, using a sticky tape to visualize mesoscale contacts. Taking into account that the apparent contact pressure in our experiment is significantly lower (0.26 and 1.9 kPa for the 0.23 and 1.77 N loads, respectively), it is surprising that the mesoscopic contact density measured in-situ in our experiments is higher for almost all tests. Perhaps differences in the measurement methodology gave differences in the area 'counted' as being in contact.

To conclude this section, it is worth noting that the mesoscopic contact area is a parameter that might be estimated with reasonable confidence from composite forming simulations. The values of mesoscopic contact area and pressure provided by the current experimental method could be used to validate such simulations.

3.2. Microscopic analysis

3.2.1. Shear angle

Fig. 7 plots histograms of the orientations of each local fibre contact identified within the macroscopic contact area, grouped by tow. The three subplots in Fig. 7 show results for progressively increased deformation, for the second shear test with a compressive force of 1.77 N. The orientations of local contacts are analysed for two tows in each of the "positive" and "negative" orientations. Fig. 7 shows that micro-contact orientations are distributed normally with a similar distribution for two parallel tows. Due to slightly unsymmetrical loading, the positive and negative tows do not deform symmetrically, giving differences in the shape of the orientation distributions. Taking the fibre orientation at the peak of each distribution as the representative tow orientation, the difference between the peak locations for positively and negatively oriented tows gives a microscopic measurement of the angle 2β between tows. The shear angle θ_{mic}, indicated on the left of each subplot, equals $90° - 2\beta$. These angles are calculated for each deformation step with all three microscopic experiments and are used in other plots to characterise the deformation.

3.2.2. Contact length

The microscopic analysis allows evaluation of the length of contact between fibres and the glass plate. To characterise the contact geometry, we define a microscopic fibre contact density D_{mic} as the ratio of the actual line contact L to that corresponding to an idealised packing geometry of parallel touching fibres over an area A. For fibres of diameter d (taken as 7 μm as specified by the manufacturer) this gives:

$$D_{mic} = \frac{dL}{A} \times 100\% \quad (2)$$

A value of D_{mic} = 100% corresponds to perfect packing of fibres at the contact plane, while a value below that indicates reduced contact between the fibres and the glass. In the following paragraphs the fibre density is defined in two ways, either with respect to the overall area of contact or as a local density based just on the tow contact patches.

The overall microcontact density $D_{mic/all}$ is given by equating the contact length in Eq. (2) as the sum of the contact lengths for all N local fibre contacts, with the normalising area taken as the total analysed area A_{mac}, to give

$$D_{mic/all} = \frac{d\sum_{i=1}^{N} L_{mic,i}}{A_{mac}} \times 100\% \quad (3)$$

The evolution of the overall contact density $D_{mic/all}$ with increasing shear angle θ_{mic} is plotted in Fig. 8. The overall contact density in all cases is less than 4%. The contact density for a compressive force of 0.23 N does not change significantly with fabric shear angle. The contact density is higher for the higher load of 1.77 N than for the lower load, decreasing with shear deformation up to

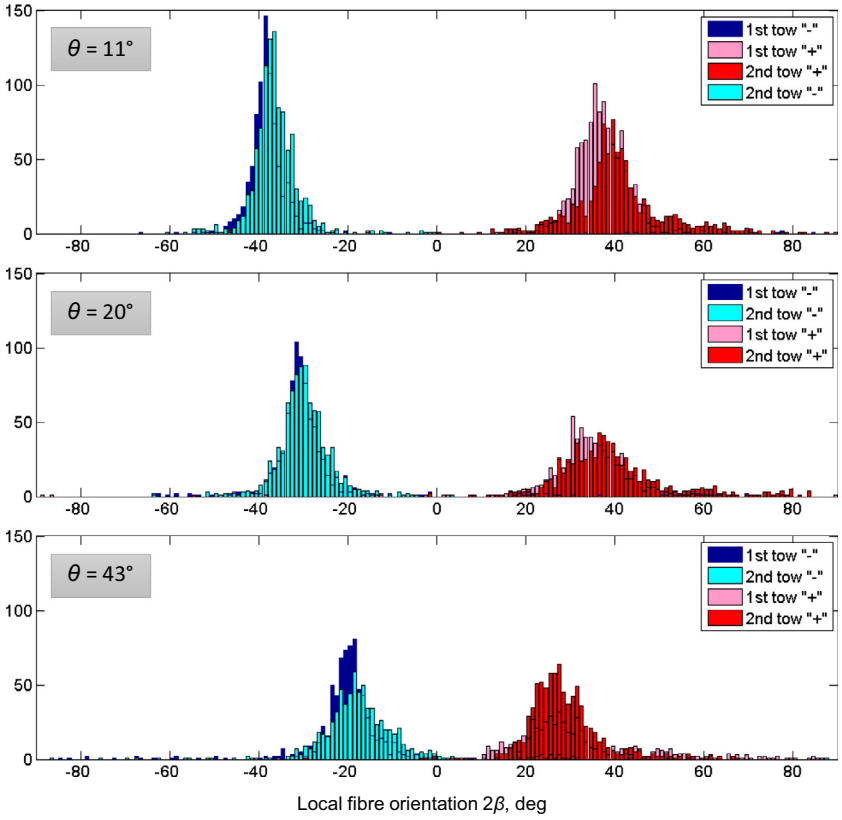

Fig. 7. Distribution of the local fibre orientation in each of the four tows within the chosen macroscopic area with a compressive load of 1.77 N.

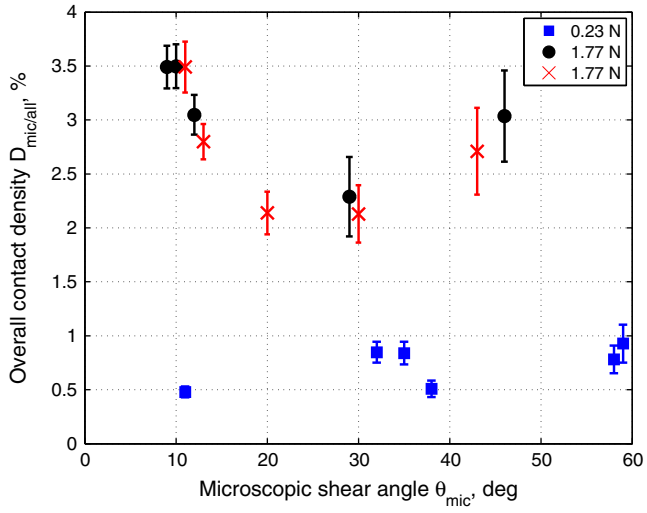

Fig. 8. Dependence of the overall micro-contact density $D_{mic/all}$ on the microscopic shear angle θ_{mic}. Error bars represent the estimated standard deviation in density associated with the limited size of the measurement area A_{mac}.

a shear angle of 30°, and then increasing almost back to its initial value. There is good repeatability for the two experiments performed at a load of 1.77 N.

In order to estimate the potential error for these measurements, the effect of the size of the analysed area A_{mac} on the accuracy of the results was investigated. Each area A_{mac} consists of nine rows of eight microscopic images. The width of this area spans the glass plate. However, only a subsection of the width of the specimen (equal to 27 rows of microscope images, with 8 images in each row, at the beginning of the experiment) is used in the analysis to reduce the observation time. To check that the reduced analysis area is sufficient, the contact areas are calculated individually for each of the nine rows in A_{mac} and the standard deviation s_1 of these nine areas found. The standard deviation of the contact area for the whole measurement area comprising all nine rows is then estimated as $s_9 = s_1/\sqrt{9}$. These standard deviations, which are taken as an estimate of the error in the measurement of contact density, are plotted as error bars in Fig. 8 and are found to be acceptable compared with the differences in contact area.

The above results normalise the contact length by the overall area. However, as noted in the previous section, the tow contact area is only a proportion of the overall area of nominal contact. Hence, to understand the local contact conditions, it is useful to calculate the micro-contact density of local fibre contacts $D_{mic/tow}$ based on the mesoscopic contact area of the four measured tows as follows

$$D_{mic/tow} = \frac{1}{4}\sum_{i=1}^{4}\frac{L_{mic,i}d}{A_{mes,i}} \times 100\% \quad (4)$$

The variation of this tow micro-contact density with microscopic shear angle θ_{mic} is plotted in Fig. 9. The mean value from four tows in each macroscopic area A_{mac} is calculated and shown in Fig. 9, with the standard deviation in the micro-contact density within these four tows shown by error bars. Fig. 9 indicates that the tow micro-contact density does not change significantly with the shear angle for the low compressive load, but decreases gradually with increasing shear angle for the higher load. The values of this tow contact density are very small, i.e. about 2–3% for the low load and between 4% and 8% for the tests with a compressive load of 1.77 N.

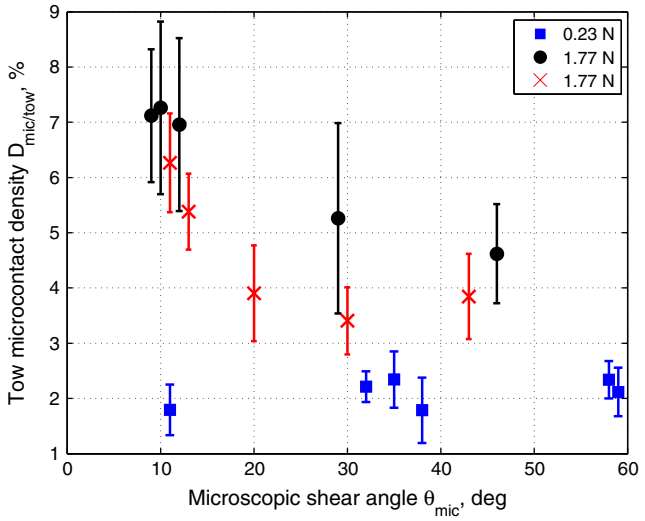

Fig. 9. Dependence of the tow micro-contact density $D_{mic/tow}$ on the microscopic shear angle θ_{mic}. Error bars represent the standard deviation of contact density for the four tows included in each measurement.

The very small values of tow micro-contact density seen in Fig. 9 indicate that the configuration of the fibres at the contact plane is far from an idealised arrangement of touching parallel fibres. This result is analogous to the case of random-packing of spheres, where there is an upper limit on density of 63.4% somewhat below the ideal close-packed value of 74% [41]. Here "jamming" leads to configurations away from the ideal arrangement of the spheres, with local friction playing an important role in controlling the behaviour.

It is also interesting to draw an analogy with soil mechanics, where the strength of soil can be understood using a model with local frictional contacts [42]. The difference between spheres or approximately equiaxed particles and the long filaments of fibre composites changes considerably the scope for non-idealised stacking associated with three-dimensional arrangement of filaments within the tow. Examination of the contact images, Fig. 3, suggests that a few randomly-oriented fibres can bridge many other fibres creating a small contact density. Taking the soil analogy further, changes in the normal contact pressure might be expected to have a relatively minor role as the frictional forces resisting the relative motion of fibres rise in conjunction with the normal forces. Furthermore reduced friction between fibres, perhaps associated with sizing or resin, could enhance conformance and so increase contact density. In fact a motivation for including fabric shearing in the current work was to examine the hypothesis that relative sliding of fibres due to fabric shear would 'break the friction' and increase the contact density. However the results do not support this hypothesis. Whatever the exact mechanisms, this discussion implies that details of the fibre configuration and of the local contact between fibres (associated both with different fibre manufacturing details and with different fabric processing conditions) might be expected to affect the contact area and hence friction conditions considerably.

3.2.3. Micro-contact area

Although the length of the fibre contacts can be measured from the microscopic images, their resolution is insufficient to give an accurate estimate of the contact width. However, assuming a circular fibre cross section (which is appropriate for the T700 fibres of this study), Hertz theory for elastic contact between a cylinder and a plane [43] provides a theoretical estimate for the width of the contact between a fibre and the glass plate. The half-width of contact a is given as

$$a = \sqrt{\frac{4dN}{2\pi E^* L_{mic}}} \tag{5}$$

where the load N over the contact patch is identical to the applied load, assuming uniform pressure over the gauge section, and the contact length L_{mic}, which varies with shear angle θ, is taken from the microscopic evaluation. The effective elastic modulus E^* is calculated from the elastic moduli E_{CF} and E_{glass} and Poisson's ratios v_{CF} and v_{glass} of the carbon fibre and glass, respectively

$$\frac{1}{E^*} = \frac{1 - v_{glass}^2}{E_{glass}} + \frac{1 - v_{CF}^2}{E_{CF}} \tag{6}$$

Values used for these calculations are $E_{glass} = 69$ GPa, $E_{CF} = 17$ GPa, $v_{glass} = 0.24$, $v_{CF} = 0.31$. Because of the loading, the average transverse modulus and Poisson's ratio of T700 carbon fibre measured by laser resonant ultrasound spectroscopy [44] are used in this expression, while standard properties are used for the glass [45]. The difficulty of measuring the transverse modulus and Poisson's ratio of carbon fibres is a source of uncertainty in the contact width estimate. In principle the contact half-width depends on the shear angle (via the contact length) and the load, but in fact the variation with these parameters is relatively small, with the estimated contact half-width taking a value of 0.0183 ± 0.0035 μm for all measurements under both loads. Although the T700 carbon fibres used in this study are rather smooth, as can be seen in AFM images [38], in general there will be nanoscale roughness on the fibre surface. Such roughness depends on the fibre type, being affected by the heat and surface treatment used for the fibre manufacture. The effect of nanoscale roughness is not taken into account in the present study, but such roughness will tend to decrease the contact area and, consequently, increase the real contact pressure.

Based on our estimates of the contact half-width and the measured microscopic contact length, the total micro-contact area A_{mic} is calculated:

$$A_{mic}(\theta) = 2L_{mic}(\theta)a(\theta) \tag{7}$$

This real contact area, averaged over the different shear angles for each load, equals 0.0094 ± 0.0013 mm^2 and 0.0519 ± 0.0005 mm^2 for the tests with compressive loads of 0.23 and 1.77 N, respectively. These real contact areas correspond to 0.003% and 0.017% of the macroscopic (nominal) overall contact area, respectively. These calculations demonstrate that, although the normal load significantly affects the real microscopic contact area, the ratio of the real to apparent contact area remains extremely small. On the other hand, the variations of real contact area with shear angle are not so important.

3.3. Contact pressures

In order to estimate macroscopic contact pressures, the experiment with a compressive load of 1.77 N was repeated a third time whilst viewed by a standard camera recording images of the whole specimen during shear. The apparent contact area A_{app} of the region of the specimen clamped between the glass plates was measured from the images, being 900 and 628 mm^2 at the start and end of the experiment, respectively. At the same time, a thickening of the specimen was measured in order to estimate the change in compression force during the test associated with the corresponding compression of the loading springs. It was found that the normal force increased from 1.77 to approximately 2.17 N, which corresponds to apparent contact pressures of 1.97 and 3.45 kPa at the start and end of the test, respectively.

Based on these values, the mesoscopic contact pressure can be calculated as

Table 1
Apparent, mesoscopic and real microscopic contact pressures calculated for the start and the end of the shear test with a compressive load of 1.77 N.

	Apparent contact pressure, p_{app} (kPa)	Mesoscopic contact pressure, p_{mes} (Eq. (8)) (kPa)	Real contact pressure, p_{mic} (Eq. (9)) (kPa)
Start of test ($\theta \approx 20°$)	1.97	3.45	30.8×10^3
End of test ($\theta \approx 50°$)	3.45	4.73	41.6×10^3

$$p_{mes}(\theta) = \frac{N(\theta)}{D_{mes}(\theta)A_{app}(\theta)} \tag{8}$$

For this estimate, D_{mes} is taken as 57% and 73% at the start and end of the test, respectively (see Fig. 6), and normal loads and apparent areas are taken from the experiment recorded by the standard camera. Substituting these values into Eq. (8), the mesoscopic contact pressures are calculated as 3.45 kPa and 4.73 kPa, respectively.

The average real contact pressure p_{mic} based on the microscopic contact area can be calculated as the ratio of the applied compression load and the total real contact area calculated using the Hertz model, giving:

$$p_{mic}(\theta) = \frac{N(\theta)}{2a(\theta)L_{mic}(\theta)} \tag{9}$$

Since the compressive load of 0.23 N was constant during the test (this load was not regulated by the springs as with the higher load, but applied only by the weight of the glass plate), the average real contact pressure can be calculated for the whole range of shear angles in this case. This equals 24.8 ± 3.65 MPa, following an inverse relationship with D_{mic} and hence changing only slightly with shear angle. The real contact pressure with a compressive force of 1.77 N can only be calculated at the start and end of the test due to a lack of continuous measurement of the normal load during the test. Considering the increase of compression load from 1.77 N to 2.17 N between the start and the end of experiment, the real contact pressure varies between 30.8 MPa and 41.6 MPa.

Apparent, mesoscopic and real contact pressures for the start and end of the test at a contact load of 1.77 N are summarised in Table 1. This table demonstrates that, while the mesoscopic contact pressure is about two times higher than the apparent pressure, the microscopic, or real, contact pressure is thousands of times higher due to the extremely small real contact area.

4. Conclusions

Information about the real contact area and real contact pressure is critical to developing tribological models of composites forming and to better design appropriate experimental measurements characterising friction. This paper describes an investigation of the true contact area at the fibre level, presenting results obtained whilst shearing of twill carbon fabric under compressive load. The main conclusions, taken from results with a compressive load of 1.77 N corresponding to a contact pressure of 1.9 kPa, are:

- the meso-scale contact density (i.e. the tow contact area relative to the nominal area) is between 55% and 75% for the whole range of shear angles considered;
- the micro-scale contact density within a tow contact (i.e. the fibre contact length relative to an idealised configuration with parallel touching fibres) is just 4–8%, indicating that the fibre arrangement at the contact is far from the idealised configuration;
- the micro-scale contact density varies significantly with fabric shear;
- the real contact area, obtained from the measured fibre contact length and using Hertz theory to estimate the contact width, is only about 0.017% of the macroscopic contact area and does not change significantly with fabric shear;
- the real contact pressure at the fibre level is estimated as about 15,000 times higher than the apparent contact pressure.

The implication of these findings is that models of tribology in composites forming and experiments characterising friction need to consider non-idealised fibre packing arrangements in any contact model. Fibre packing and hence tribological conditions may be influenced strongly by details such as fibre material, tow manufacturing details, fibre sizing, the presence of resin and resin pressure.

Acknowledgments

The authors are very grateful to the Tribology groups of the LTDS laboratory in Lyon and Imperial College, London for help with the semi-reflective coatings. We also acknowledge the contribution of our industrial partners Jaguar Land Rover and Granta Design Ltd, as well as the academic partners from the Composites group at the University of Nottingham. This work was funded by an Engineering and Physical Sciences Research Council grant (reference EP/K032798/1).

References

[1] Long AC. Composites forming technologies. Cambridge: Woodhead; 2007.
[2] Lomov SV. Non-crimp fabric composites: manufacturing, properties and applications. Cambridge: Woodhead; 2011.
[3] Advani S, Hsiao KT. Manufacturing techniques for Polymer Matrix Composites (PMCs). Cambridge: Woodhead; 2012.
[4] Buet-Gautier K, Boisse P. Experimental analysis and modeling of biaxial mechanical behavior of woven composite reinforcements. Exp Mech 2001;41(3):260–9.
[5] Nestor TA, O Bradaigh CM. Experimental investigation of the intraply shear mechanism in thermoplastic composites sheetforming. Key Eng Mater 1995;99–100:19–36.
[6] Harrison P, Clifford MJ, Long AC. Shear characterisation of viscous woven textile composites: a comparison between picture frame and bias extension experiments. Compos Sci Technol 2004;64(10–11):1453–65.
[7] Stanley WF, Mallon PJ. Intraply shear characterisation of a fibre reinforced thermoplastic composite. Compos Part A: Appl Sci 2006;37(6):939–48.
[8] Hivet G, Duong AV. A contribution to the analysis of the intrinsic shear behavior of fabrics. J Compos Mater 2011;45(6):695–716.
[9] Lomov SV, Willems A, Verpoest I, Zhu Y, Barburski M, Stoilova T. Picture frame test of woven composite reinforcements with a full-field strain registration. Text Res J 2006;76(3):243–52.
[10] Cao J, Akkerman R, Boisse P, Chen J, Cheng HS, de Graaf EF, et al. Characterization of mechanical behavior of woven fabrics: experimental methods and benchmark results. Compos Part A: Appl Sci 2008;39(6):1037–53.
[11] Verpoest I, Lomov SV. Virtual textile composites software WiseTex: integration with micro-mechanical, permeability and structural analysis. Compos Sci Technol 2005;65(15–16):2563–74.
[12] Blacklock M, Bale H, Begley M, Cox B. Generating virtual textile composite specimens using statistical data from micro-computed tomography: 1D tow representations for the Binary Model. J Mech Phys Solids 2012;60(3):451–70.
[13] Boisse P, Zouari B, Gasser A. A mesoscopic approach for the simulation of woven fibre composite forming. Compos Sci Technol 2005;65(3–4):429–36.
[14] Aimene Y, Hagege B, Sidoroff F, Vidal-Sallé E, Boisse P, Dridi S. Hyperelastic approach for composite reinforcement forming simulations. Int J Mater Form 2008;1:811–4.
[15] Hamila N, Boisse P, Chatel S. Finite element simulation of composite reinforcement draping using a three node semi discrete triangle. Int J Mater Form 2008;1(1):867–70.
[16] Badel P, Vidal-Sallé E, Maire E, Boisse P. Simulation and tomography analysis of textile composite reinforcement deformation at the mesoscopic scale. Compos Sci Technol 2008;68(12):2433–40.
[17] Chen QQ, Boisse P, Hamila N, Saouab A, Park CH, Bréard J. A finite element method for the forming simulation of the reinforcements of thermoplastic composite. Int J Mater Form 2009;2:213–6.

[18] ten Thije RHW, Akkerman R. A multi-layer triangular membrane finite element for the forming simulation of laminated composites. Compos Part A: Appl Sci 2009;40(6):739–53.
[19] Vanclooster K, Lomov SV, Verpoest I. Simulation of multi-layered composites forming. Int J Mater Form 2010;3:695–8.
[20] Durville D. Simulation of the mechanical behaviour of woven fabrics at the scale of fibers. Int J Mater Form 2010;3(2):1241–51.
[21] Miao Y, Zhou E, Wang Y, Cheeseman BA. Mechanics of textile composites: micro-geometry. Compos Sci Technol 2008;68(7–8):1671–8.
[22] Gorczyca JL, Sherwood JA, Liu L, Chen J. Modeling of friction and shear in thermostamping of composites-Part I. J Compos Mater 2004;38(21): 1911–29.
[23] Hermann D, Ramkumar SS, Seshaiyer P, Parameswaran S. Frictional study of woven fabrics: the relationship between the friction and velocity of testing. J Appl Polym Sci 2004;92(4):2420–4.
[24] Das A, Kothari VK, Vandana N. A study on frictional characteristics of woven fabrics. Autex Res J 2005;5(3):133–40.
[25] Ersoy N, Potter K, Wisnom MR, Clegg MJ. An experimental method to study the frictional processes during composites manufacturing. Compos Part A: Appl Sci 2005;36(11):1536–44.
[26] ten Thije RHW, Akkerman R, van der Meer L, Ubbink MP. Tool–ply friction in thermoplastic composite forming. Int J Mater Form 2008;1(1):953–6.
[27] ten Thije RHW, Akkerman R. Design of an experimental setup to measure tool–ply and ply–ply friction in thermoplastic laminates. Int J Mater Form 2009;2(1):197–200.
[28] Fetfatsidis KA, Jauffrès D, Sherwood JA, Chen J. Characterization of the tool/fabric and fabric/fabric friction for woven-fabric composites during the thermostamping process. Int J Mater Form 2013;6(2):209–21.
[29] Cornelissen B, Rietman B, Akkerman R. Frictional behaviour of high performance fibrous tows: friction experiments. Compos Part A: Appl Sci 2013;44(1):95–104.
[30] Harrison P, Lin H, Ubbink M, Akkerman R, Van De Haar K, Long AC. Characterising and modelling tool–ply friction of viscous textile composites. In: ICCM Int Conf Compos Mater; 2007.
[31] Najjar W, Pupin C, Legrand X, Boude S, Soulat D, Dal Santo P. Analysis of frictional behaviour of carbon dry woven reinforcement. J Reinf Plast Compos 2014;33(11):1037–47.
[32] Bowden FP, Tabor D. The area of contact between stationary and between moving surfaces. Proc R Soc Lond A Math 1939;169(938):391–413.
[33] Cornelissen B, de Rooij MB, Rietman B, Akkerman R. Frictional behaviour of high performance fibrous tows: a contact mechanics model of tow-metal friction. Wear 2013;305(1–2):78–88.
[34] Chang SH, Sharma SB, Sutcliffe MPF. Microscopic investigation of tow geometry of a dry satin weave fabric during deformation. Compos Sci Technol 2003;63(1):99–111.
[35] Chang SH, Sutcliffe MPF, Sharma SB. Microscopic investigation of tow geometry changes in a woven prepreg material during draping and consolidation. Compos Sci Technol 2004;64(10–11):1701–7.
[36] Smedova O, Sutcliffe MPF. Novel experimental method for microscale contact analysis in composite fabric forming. Experimental Mechanics 2014 [submitted for publication].
[37] Smerdova O, Sutcliffe MPF. Tribological study of polymer composite forming using model experiments and real composites. Key Eng Mater 2014;611–612:300–5.
[38] Cornelissen B, Sachs U, Rietman B, Akkerman R. Dry friction characterisation of carbon fibre tow and satin weave fabric for composite applications. Compos Part A: Appl Sci 2014;56:127–35.
[39] Chen B, Chou T-W. Compaction of woven-fabric preforms in liquid composite molding processes: single-layer deformation. Compos Sci Technol 1999; 59(10):1519–26.
[40] Nguyen QT et al. Mesoscopic scale analyses of textile composite reinforcement compaction. Compos Part B: Eng 2013;44(1):231–41.
[41] Song C, Wang P, Makse HA. A phase diagram for jammed matter. Nature 2008;453(7195):629–32.
[42] Powrie W. Soil mechanics: concepts and applications. 2nd ed. Spon: Abingdon (Oxon); 2004.
[43] Johnson KL. Contact mechanics. Cambridge: Cambridge University Press; 1987.
[44] Mounier D, Poilâne C, Bûcher C, Picart P. Evaluation of transverse elastic properties of fibers used in composite materials by laser resonant ultrasound spectroscopy. Société Française d'Acoustique. Acoust 2012 2012 [Nantes, France].
[45] Edupack CES. Granta Design Ltd., Cambridge; 2014.